JACS
JOURNAL OF THE AMERICAN CHEMICAL SOCIETY
pubs.acs.org/JACS
Article

On the Control of Directionality of Myosin

Ritaban Halder, Zhen Tao Chu, Rujuan Ti, Lizhe Zhu, and Arieh Warshel*

Cite This: J. Am. Chem. Soc. 2024, 146, 28360−28374
Read Online
ACCESS | Metrics & More | Article Recommendations | Supporting Information

ABSTRACT: The origin of the unique directionality of myosin has been a problem of fundamental and practical importance. This work establishes in a conclusive way that the directionality is controlled by tuning the barrier for the rate-determining step, namely, the ADP release step. This conclusion is based on exploring the molecular origin behind the reverse directionality of myosins V and VI and the determination of the origin of the change in the barriers of the ADP release for the forward and backward motions. Our investigation is performed by combining different simulation methods such as steer molecular dynamics (SMD), umbrella sampling, renormalization method, and automated path searching method. It is found that in the case of myosin V, the ADP release from the postrigor (trailing head) state overcomes a lower barrier than the prepowerstroke (leading head) state, which is also evident from experimental observation. In the case of myosin VI, we noticed a different trend when compared to myosin V. Since the directionality of myosins V and VI follows a reverse trend, we conclude that such differences in the directionality are controlled by the free energy barrier for the ADP release. Overall, the proof that the directionality of myosin is determined by the activation barrier of the rate-determining step in the cycle, rather than by some unspecified dynamical effects, has general importance.

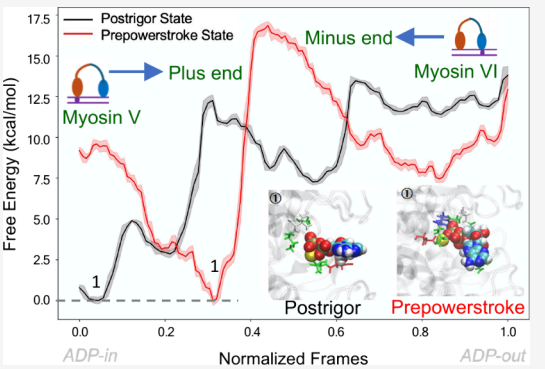

1. INTRODUCTION

Myosin is a class of motor proteins that are involved in muscle contraction, cell migration, and intracellular transport.[1] They generally move along the actin filaments and always utilize ATP hydrolysis to generate force and movement. Kinesins are another class of motor proteins, which move along microtubules, and they carry cargo such as organelles, protein complexes, and vesicles toward different compartments inside the cell.[2,3] Another important class of motor proteins is dynein, which also moves along microtubules but in the reverse direction of kinesin. They are involved in several intracellular transports and flagellar movements, and positioning of organelles for their proper functions.[4,5] It is important to note that although the mechanisms of action of these motor proteins could differ, in all the cases, the ATP hydrolysis and subsequent release of the hydrolyzed products (ADP and Pi) govern a cycle of processes that occur along the track (either on the actin filament or on the microtubule) of these motor proteins, which results in force generation and their movement in a specific direction.[6]

Motor proteins play essential roles in the maintenance of cellular structure and function. Dysfunctions or mutations in motor proteins can lead to various lethal diseases and physiological disorders, including developmental abnormalities, neurodegenerative diseases, and certain types of cancer.[7−9] For example, the absence of myosin Va in human often leads to a severe neurological disease called Griscelli syndrome.[10] Mutation of myosin VI causes deafness in mammals.[11,12] Mutations in kinesin often leads to motor neuron disease.[13] Dynein mutation could result Alzheimer's disease and spinal muscular atrophies.[14,15] Thus, proper understanding of the mechanisms of action and the regulation of motor proteins is crucial and of pivotal importance for biomedical research and the development of therapeutic targets.

Motor proteins also play a vital role behind the muscle contraction and are responsible for the active transport of most proteins and vesicles in the cytoplasm. The directionality of the movement of the motor protein is very important.[16,17] Kinesin moves toward the plus end of the cell,[18] whereas dynein moves toward the minus end of the cell.[19] All the myosin family proteins move toward the plus end of the cell, except myosin VI, which moves toward the minus end. Structurally, myosin consists of a head domain (consists of two motor heads in general), which is often termed the catalytic motor domain, followed by the neck domain with which the tail domains are bound. Figure 1 shows a schematic representation of a dimeric myosin motor walking on the actin filaments. Myosin carries cellular cargo from one end to another end of the cell along the

Received: July 14, 2024
Revised: September 17, 2024
Accepted: September 18, 2024
Published: October 5, 2024

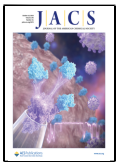

https://doi.org/10.1021/jacs.4c09528
J. Am. Chem. Soc. 2024, 146, 28360−28374

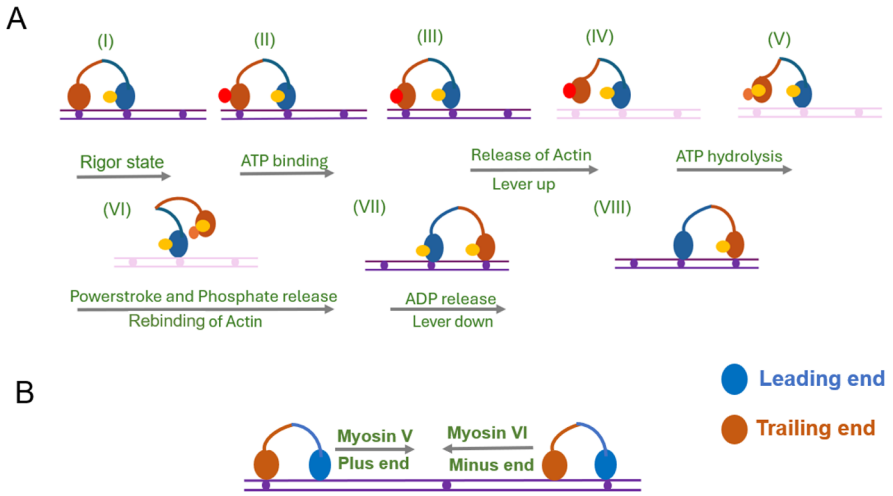

Figure 1. Schematic diagram of the mechanochemical cycle of myosin. (A) Walking mechanism for a single step of myosin motor dimer over the actin filament in the forward direction. The cycle starts with the attachment of the double-headed myosin to the actin track, where one of the myosin heads is bound with ADP (Figure 1A, step I). Next, the ATP molecule binds with a motor head domain (Figure 1A, steps II–III). The ATP bound motor head becomes loosely associated from the actin track and motor head switch to a lever-up conformation (Figure 1A, step IV). Then, the motor head with bound ATP hydrolyzed to produce ADP and phosphate (Figure 1A, step V). Next, the power stroke state begins as loss of the phosphate (Pi) ion is assumed to initiate the onset of the power stroke (Figure 1A, VI), and it leads to strong binding of the motor protein with the actin filaments. After phosphate release, bound ADP has also been released from the myosin head (Figure 1A, VII) and now myosin goes to a lever-down conformation. This ADP release step is the slowest step of the cycle and controls the overall rate of the whole cycle. Finally, myosin steps forward by this way (Figure 1A, VIII) and carries cellular materials toward its destination. The cycle continues until the myosin completes its function of cellular transport. (B) Representation of the directionality of myosin V and myosin VI dimer. During their action, myosin V walks toward the plus end, whereas myosin VI moves toward the minus end.

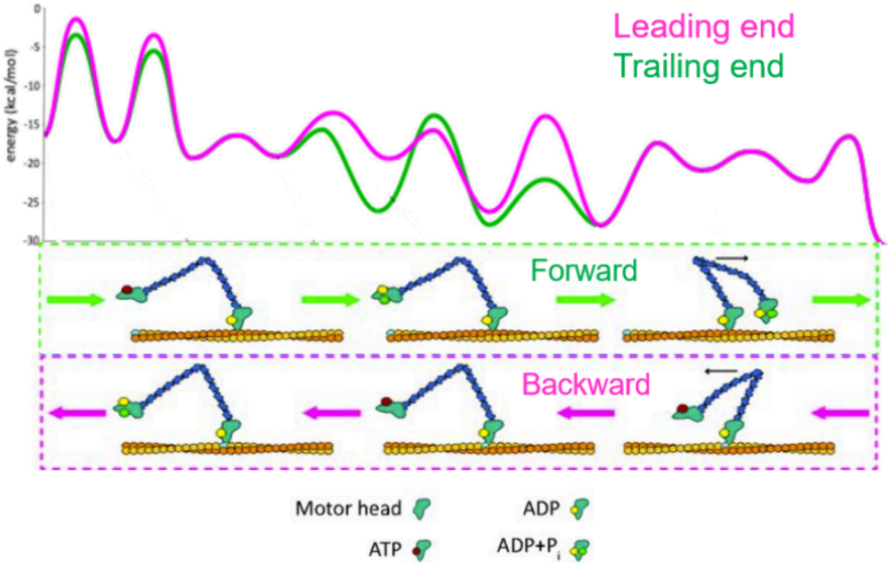

Figure 2. Free energy landscape for myosin stepping. In this landscape, the forward step is shown in green and the backward step in pink. The rate-determining step is the ADP release step, which has a higher barrier for the backward motion. The corresponding forward and backward steps are illustrated at the bottom of the plot. Note that the motor head, ADP, ATP, and ADP+P_i are marked by specific notations as indicated by different shapes in the figure. The actin filament is shown by small beads just beneath the motor head. The myosin dimer inside the green dotted box is involved in a forward movement, whereas the myosin dimer inside the pink dotted box is involved in a backward movement.

actin track. It always utilizes ATP during its action. The complete myosin mechanochemical cycle is depicted in Figure 1A. It starts with the attachment of the double-headed myosin to the actin track where one of the myosin heads is bound with ADP (Figure 1A, step I). A specific interaction between myosin and actin leads to a strong binding between them. Then, the ATP molecule binds with a motor head domain (Figure 1A, steps II–III). Then, the ATP-bound motor head becomes loosely associated from the actin track, and conformational change triggers the motor head to switch to a lever-up conformation (Figure 1A, step IV). Then, the motor head with bound ATP was hydrolyzed to produce ADP and phosphate (Figure 1A, step V). Next, the power stroke state begins as loss of the phosphate (Pi) ion is assumed to initiate the onset of the power stroke (Figure 1A, VI) and also leads to strong binding of the motor protein with the actin filaments. After phosphate release, bound ADP has also been released from the myosin head (Figure 1A, VII) and now myosin goes

https://doi.org/10.1021/jacs.4c09528
J. Am. Chem. Soc. 2024, 146, 28360–28374

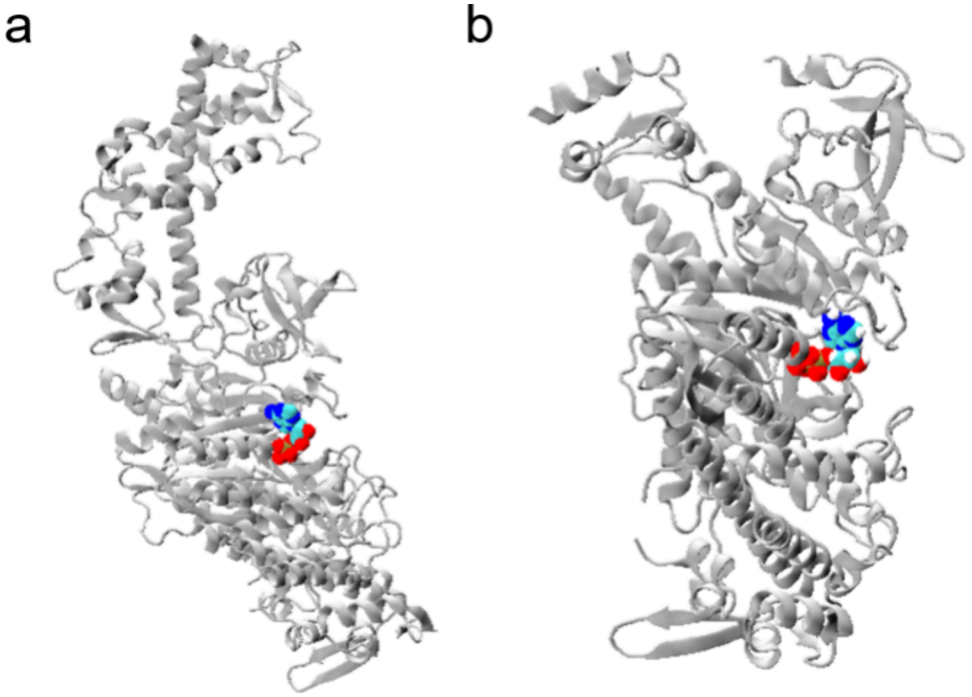

Figure 3. Structures of myosin V in a cartoon representation. (a) Postrigor state of myosin V. The attached ADP is shown by vdW representation. (b) Prepowerstroke state of myosin V with ADP. The structures of postrigor conformation and prepowerstroke conformation have been taken from the protein data bank having PDB ID 1w7j.pdb and 4zg4.pdb, respectively.

to a lever-down conformation. This ADP release step is the slowest step of the cycle and controls the overall rate of the whole cycle. Finally, myosin steps forward by this way (Figure 1A, VIII) and carries cellular materials toward its destination. The cycle continues until myosin completes its function of cellular transport. It is worth mentioning that the binding of ATP could trigger dissociation of the myosin-actin bound complex, and the hydrolysis of ATP then induces a conformational change in myosin.

Many experimental and computational studies have been focused on myosin, attempting to find out its function and activity at different conditions.[11,12,20−25] For example, recent experimental studies have involved significant progress in understanding the mechanochemical cycle of myosin. Single-molecule experiments reveal that certain single-point mutations in myosin could trigger its functional activity by altering the ADP dissociation rate from myosin, which in turn affects the duty ratio of myosin.[11,12] The kinetic study of the single-headed myosin motor suggested that ADP release from the head domain is the rate limiting step in the whole cycle.[26] The weak binding states of myosin V have also been probed by several kinetic experiments.[27] It is important to note in this context that investigations of myosin motors at different nucleotide bound states as well as in inactive states have refined our understanding on that subject significantly. Smith and Sleep investigated the strain-dependent kinetics of myosin using optical trap experiments.[28] From kinetic experiments, Trybus and co-workers[29] concluded that monomeric myosin V could also be processive. Cappello et al.[20] studied the stepping mechanism of myosin V experimentally using optical tweezers. Other experimental studies provided evidence behind the head-to-head coordination between the two head domains of myosin motors when they are at the dimeric states.[30]

Theoretical and computational techniques have also demonstrated progress on many aspects of the myosin motor. The actin-myosin organization has been studied by simulation.[31] Using computational techniques, scientists have explored the dynamics of the motor processivity,[32] transition between different states of the cycle,[33] and coupling between several parts of the motor domain.[34] Masuda et al.[35] studied the interaction between actin filament with myosin by means of molecular dynamics (MD) simulations. Coarse-gained modeling of the mechanochemical cycle has also been performed in order to elucidate the behavior of these proteins.[22,23]

Despite the above studies, most works have not addressed what is argutely the most interesting problem, namely, the reason for the unidirectionality of the motion of myosin. In fact, the tendency has been to assume that this unique feature is due to a dynamical effect, which is presumably associated with the powerstroke. The most direct studies that address this problem were reported in our works[22,23] that culminated in the work described in ref 22, where it was concluded that the directionality is determined by the difference in the barrier for the ADP release step for the forward and backward motions, as shown in Figure 2. This means that the directionality is controlled exquisitely by the free energy of rate determining barriers and not by some dynamical factors. This point has already been established in ref 22 but was not confirmed by careful free energy calculations. While our previous study provides compelling support to the idea that the directionality is controlled by the energetics of rate-determining steps, it does not seem that this idea has been widely accepted. Thus, we focused in this work on quantifying the structure/energetics analysis of the ADP release step in myosins V and VI. Furthermore, we examined how the different conformational states of myosin V and VI motors affect the energetics of the key rate-limiting ADP release states and lead to motions in the opposite directions. Using multiple approaches, we have found that ADP release from the trailing head of myosin V follows a

https://doi.org/10.1021/jacs.4c09528
J. Am. Chem. Soc. 2024, 146, 28360−28374

lower activation barrier compared to the ADP release from the leading head. It is important to note that experimental observations also lead to similar findings in terms of rate constants but do not prove that the rate constants reflect the activation free energies. On the other hand, in the case of myosin VI, we have found that the ADP release energetics follows a different trend. It has been found that the activation barrier for the release of ADP from the trailing head of myosin VI is higher than that for the leading head. Since myosins V and VI (Figure 1B) are operated in opposite directions, the observed reverse trend in the ADP release energetics from myosins V and VI is a definite contributor to their different directionality.

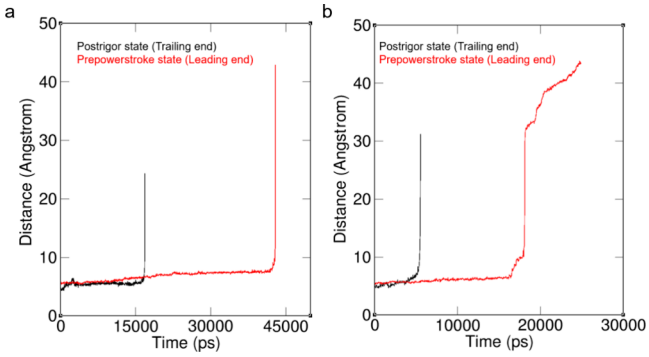

Figure 4. SMD simulation results of Myosin V. The Myosin-ADP distance has been plotted as a function of time. At lower distance, the ADP and Myosin are attached to each other whereas at higher distance they are dissociated from each other. a: SMD results of ADP dissociation from Myosin V at postrigor and prepowerstroke conformation at a force constant 0.004 kcal mol^{-1} Å^{-2} and b. SMD results of ADP dissociation from Myosin V at postrigor and prepowerstroke conformation at a force constant 0.009 kcal mol^{-1} Å^{-2} at postrigor and prepowerstroke conformation.

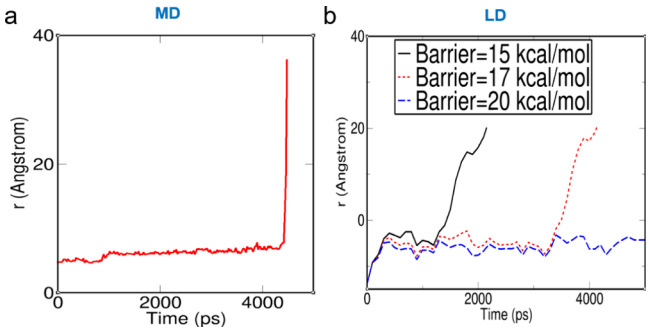

Figure 5. Renormalization simulations for ADP binding and unbinding to myosin V (trailing end, postrigor state). The 1D LD model with a force constant of 0.02 kcal mol^{-1} Å^{-2} and friction of 50 ps^{-1} with varying barriers (ΔG = 15, 17, and 20 kcal/mol) is compared to the explicit TMD (a). This was done until the characteristic passage times for that force constant in LD (b) are consistent with those obtained from the MD passage times. We observed that the behavior closest to the explicit model is recreated at an activation barrier around the 17 kcal/mol range and a friction of 50 ps^{-1}.

2. METHODS

In order to establish the nature of the rate-determining barrier, we decided to use different simulation approaches and thus to gain confidences about the calculated results despite the major convergence problems. Although some of the approaches used here may not provide correct absolute barriers, we will try to see if they give the correct trend in differences between the barriers for ADP release. The methods used are described in the following.

2.1. SMD Simulation Protocol. The SMD simulation technique can provide a way to explore trends in binding energies in a very qualitative way.[36,37] Thus, we started by utilizing this protocol[38] in exploring the ADP binding/unbinding process in myosin V and myosin VI. In the case of myosin V, the ADP is closely bound to crucial myosin residues (residue 166 to 170 of myosin V, PDB ID 1w7j[39] for the postrigor state and PDB ID 4zg4[40] for the prepowerstroke state). Thus, we have monitored the center of mass distance between the ADP molecule and the center of mass distance between residues 166−170 to check ADP binding and unbinding with myosin V. In the case of myosin VI, as evident from their crystal structure, residues 156−160 are bound with the ADP molecule (PDB ID 2vb6[41] for the postrigor state and PDB ID 2v26[42] for the prepowerstroke state). Thus, we used the center of mass distance between ADP and the center of mass distance for residues 156−160 of myosin to check the binding/unbinding of ADP from myosin VI in the SMD simulations. We have performed all-atom MD simulation by utilizing GROMACS (version 2020) software,[43] and the CHARMM36 force field[44] was used for these all-atom MD simulations. The hydrogen atoms were added to the proteins using the "pdb2gmx" protocol in GROMACS. The parameters for ADP were generated by using the CHARMM General Force Field (CGenff) tool.[45] The ADP-bound myosin was first subjected to an energy minimization by using the steepest descent algorithm. Then, this energy-minimized structures were solvated using the SPC/E water model[46] in a cubic box. In all the simulations, we used periodic boundary conditions for the simulations. Before the start of all the simulations, the systems were made charge neutral by adding an appropriate number of counterions. The solvated system was then subjected to an energy minimization. All the systems were subjected to 1 ns of position-restrained dynamics using an NPT ensemble, where the protein was constrained by using a restraining force of 2.5 kcal mol^{-1} Å^{-2} for 1 ns, and all the surrounding water molecules were allowed to move independently. After those position-restraint simulations, we performed the actual SMD production simulations with those systems. Different force constants (0.004 and 0.009 kcal mol^{-1} Å^{-2}) were used for each of our systems to check the relative trend in the forward and backward barriers, which is reflected in the time of the ADP release. The pulling forces on the ADP were implemented in all directions to pull the ADP away from myosin. The system was solvated inside a cubic box filled with water, which ensures good enough solvation of myosin by water molecules. The particle mesh Ewald method was used to handle the electrostatic interactions. The temperature and pressure of those systems were maintained by using Nosé−Hoover thermostat[47,48] and Parrinello−Rahman barostat,[49] respectively. Each of the trajectories was saved at every 20 PS interval, and we used a time step of 0.001 PS for all these simulations.

2.2. Using the Renormalization Approach to Convert Targeted Molecular Dynamics (TMD) to Reliable Activation Barriers. Obviously, the SMD is not a sufficiently reliable approach, since it does not tell us about the actual activation barrier. Fortunately, we have a way to convert TMD results to relevant free energy results by using the renormalization approach.[50,51] This approach starts with SMD of the full explicit atomistic model of the system and then maps the results to a simple low-dimensional Langevin dynamics (LD) model that is adjusted to reproduce the energetics and dynamics of the full model. More specifically, we start with a full model that is treated by regular all-atom explicit MD simulations, where the system is forced to move in a relatively short time from the initial to the final state by different constraint forces. Next, we try to reproduce the same dynamics obtained for the explicit model by the 1D or 2D LD model with the same constraint forces and different activation barriers. We also use an effective friction that is also adjusted to give the best fit between the explicit and LD models or adjusted by reproducing the best agreement to the explicit model. The activation barrier of the LD model that provides the best fit

https://doi.org/10.1021/jacs.4c09528
J. Am. Chem. Soc. 2024, 146, 28360−28374

between the time dependence of the LD model and the explicit model is taken as the activation barrier of the explicit model. For our case, the ADP bound state with myosin is the starting state, and the final state is when ADP becomes completely unbound from myosin. Our procedure is described in more detail in our previous studies.[50,51]

2.3. Calculations of Free Energy Barriers by Umbrella Sampling Simulation. Umbrella sampling simulation offers (in principle) a way to study the free energy along conformational paths, including studies of ligand binding/unbinding to different proteins and biomolecules.[52−55] Of course, the reliability depends on the convergence, which requires a major computer time. To gain a thermodynamic insight behind ADP binding/unbinding at different conformations of myosins V and VI, we have carried out umbrella sampling simulation[56] with different conformations of myosin bound with ADP. To monitor the ADP binding/unbinding process, we used the distance between specific ADP binding residues of myosin and the center of mass of the ADP as the reaction coordinate for the umbrella sampling simulation process. The conformations of the postrigor state (trailing end) and the prepowerstroke state (leading end) of myosin motors are the most important, and we considered these states for our simulations.[22] The structure corresponds to the postrigor states, and the prepowerstroke states of myosin V have been collected from the crystal structure in the protein data bank having the PDB ID 1w7j.pdb and 4zg4.pdb, respectively. For myosin VI, the postrigor and prepowerstroke conformations have been taken from the available crystal structure of the Protein Data Bank having the PDB accession codes 2vb6.pdb and 2v26.pdb, respectively. In the crystal structure of myosin V, ADP is closely bound to crucial myosin residues (residues 166 to 170 of myosin V), and we have used the center of mass distance between the ADP molecules and the center of mass distance of residues 166−170 as an order parameter for free energy calculation. In the case of myosin VI, as evident from their crystal structure, residues 156−160 are bound with the ADP molecule. Thereafter, we used the center of mass distance between ADP and the center of mass distance of residues 156−160 as an order parameter for the free energy calculation. The distance between ADP and these residues of myosin is lower when ADP is bound to myosin, whereas they are higher when ADP becomes dissociated from myosin. In the free energy analysis, we have varied the distance between those residues of myosin and ADP from 3 to 30 Å with a small interval of 1 Å, such that we achieved sufficient sampling that leads to a converged free energy profile. Inside each umbrella sampling window, we performed 10 ns of equilibration simulations, followed by 10 ns of production simulations. In each of the umbrella sampling simulation window, we used a force constant of 0.004 kcal mol^{-1} $Å^{-2}$ to sample different states of all the systems. As in the SMD simulation, we also tested umbrella sampling simulations with different force constants, and all of them lead to qualitatively similar outcomes. The starting structures for each of the umbrella sampling simulation windows have been extracted from the SMD simulation trajectories. We have sampled all binding and unbinding events, starting from an ADP bound state to an unbound state of myosin. Next, the weighted histogram analysis method (WHAM)[57] was performed with all those simulated umbrella sampling windows to construct the free energy profile.

2.4. Automated Path Searching Method. The traveling-salesman-based automated path searching (TAPS) approach[58] is a highly efficient automated path searching method that can successfully locate the minimum free energy paths (MFEPs) for biomolecular systems with hundreds of residues at the cost of submicrosecond simulation.[59−62] TAPS only requires a distance metric, i.e., the set of atoms used to compute the root mean square distance (RMSD) between any pair of conformations, as input. To further investigate ADP binding/unbinding at different conformations of myosin V, we have carried out TAPS simulations with the postrigor state (PDB ID 1w7j.pdb) and the prepowerstroke state (PDB ID 4zg4.pdb) of myosin V, respectively. We have also performed TAPS simulations with the postrigor state (2vb6.pdb) and prepowerstroke state (2v26.pdb) of myosin VI.

TMD was first carried out using GROMACS and PLUMED-2.5.3,[63] pulling ADP or MG-ADP out of the two conformational states. The spring force constant was set to 6 kcal/(mol·$Å^2$), biasing on heavy atoms of ADP or MG-ADP, with structure alignments performed on the C-alpha atoms of the nonloop parts of the protein. TAPS was then performed via an in-house python script incorporating GROMACS, PLUMED, and Concorde[64] to find the MFEP closest to the TMD paths.[64] The simulations were performed in the NVT ensemble at 310 K, using the velocity-rescale thermostat.[65] The initial path was obtained by selecting conformations with a gap of 1.0 Å from the TMD trajectory. The RMSD between the conformations was computed using all heavy atoms of ADP or MG-ADP and their surrounding residues within 4 Å, while structure alignments were performed using C-alpha atoms of the nonloop parts of proteins. In each TAPS iteration, 1000 PS sampling was performed in total. Gaussians of height 0.05 kcal/mol and width 0.5 were deposited every 0.02 PS, with frames recorded at the same frequency. Convergence was evaluated by multidimensional scaling (MDS)[66] and PCV-z analysis.[67] A PCV-z convergence test for TAPS simulations has been added (Figure S1). All the paths used to perform the free energy calculations reached convergence in TAPS optimizations. After the optimization, free energy profiles along the MEFPs were calculated through umbrella sampling. The sampling in each 0.5 Å window was restrained within 1.5 Å of MFEP through a harmonic wall potential with a force constant of 4800 kcal/(mol$Å^2$) at PCV-z = 2.25 $Å^2$. The atom sets for alignment and RMSD calculation were the same as in the TAPS optimization. We used all the possible neighboring residues along the reference path in each iteration of TAPS and kept updating the list of neighbor residues after one iteration. Thus, the selected atoms are not just the ones in a specific conformation. We visualize the atoms for RMSD definition in Figure S2. For each window, a force constant of 48 kcal mol^{-1} $Å^{-2}$ was employed. Each window was simulated for at least 10 ns. Complete free energy profiles were evaluated with the weighted histogram analysis method (WHAM).

3. RESULTS AND DISCUSSION

3.1. SMD Simulation of Myosin V. To understand how ADP dissociation occurs from different states of myosin V (Figure 3), we first performed SMD simulation and monitored the distance between ADP and myosin V with time (Figure 4). As mentioned earlier, we considered both the postrigor and prepowerstroke conformations of myosin V to understand the ADP dissociation from myosin V. As shown in Figure 4, at lower distances, ADP is bound with myosin, whereas as

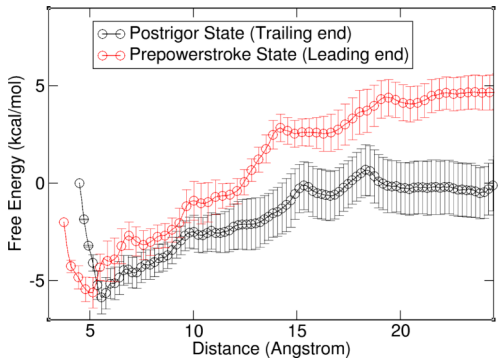

Figure 6. Umbrella sampling simulation results of myosin V at the postrigor and prepowerstroke conformations. Here, free energy is plotted by considering the distance between ADP molecule and myosin as an order parameter. At the most favorable state, the free energy minima indicate the ADP bound state to myosin whereas at higher distances, they become dissociated from each other. Note that the postrigor state has a lower energy barrier from ADP bound (to myosin) to the ADP dissociated state whereas the prepowerstroke state has a higher energy barrier. The error bars were calculated by bootstrapping.

https://doi.org/10.1021/jacs.4c09528
J. Am. Chem. Soc. 2024, 146, 28360−28374

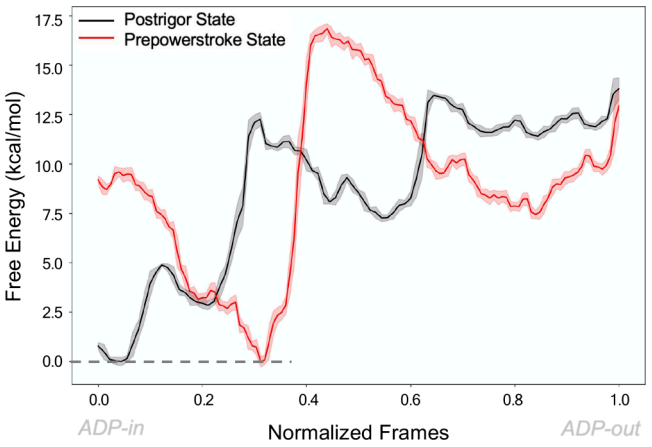

Figure 7. TAPS results for the ADP release from the postrigor and prepowerstroke states of myosin V. The *x*-axis is labeled by normalized simulation frame numbers. The "zero" value corresponds to the ADP-bound state, and the "one" value corresponds to the ADP-unbound state. The error bars are shown as transparent bands. The free energy barrier for releasing ADP in the postrigor state is lower compared to the prepowerstroke state.

distance increases, ADP gets dissociated from myosin. We have found that in the case of myosin V, ADP release is faster from the postrigor conformation whereas it is slower from the prepowerstroke conformation of myosin V (Figure 4a,b). We found qualitatively similar trends at different force constants used in this study (Figure 4). It indicates that ADP dissociates much easily from the postrigor state of myosin V compared to its prepowerstroke conformation (Supplementary Movies 1 and 2). It is important to note that a faster ADP dissociation from the postrigor state of myosin V compared to its prepowerstroke state has also been hinted from experimental findings.[21,40] Therefore, our SMD results support experimental findings. However, to acquire a detailed energetic insight of the ADP dissociation from these states, we have accomplished free energy analysis in the next sections.

3.2. Renormalization Calculations. Using pulling forces and varying barriers, we parametrize the effective barrier for the LD treatment to maximize the agreement between the time-dependent responses of both the explicit and implicit models. Applying this approach to the myosin systems, we performed LD simulations (with varying ADP release barriers for the trailing end of myosin V, as shown in Figure 5), near the barrier obtained from our TAPS simulations of respective myosin systems and with an LD force constant of 0.02 kcal mol^{-1} $Å^{-2}$ (similar to our MD force constants) for the leading end of myosin V. The optimal friction was taken here as 50 ps^{-1}. The results from our analysis are shown in Figure 5 and Supporting Information Figure S3. We found a significant overlap between the TMD result (Figure 5a) with corresponding LD results (Figure 5b) at a similar force constant between all-atom explicit MD and implicit LD at a barrier in the 17 kcal/mol range.

3.3. Umbrella Sampling Simulation of Myosin V. The renormalization simulations indicated that ADP release from the postrigor state is more feasible than the prepowerstroke state of myosin V. To get a much more reliable estimate of the energetics of the ADP release steps, we have performed

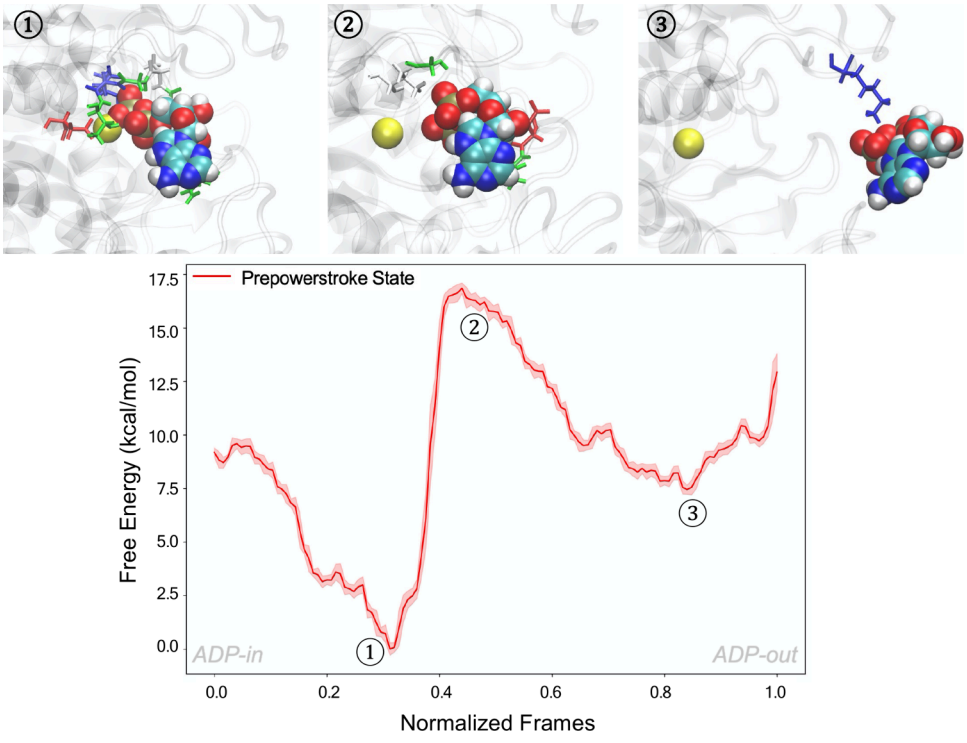

Figure 8. TAPS free energy profile along the minimum free energy path of ADP release from the prepowerstroke state of myosin V. The *x*-axis is labeled by normalized simulation frame numbers of the MFEP, with error bars shown as transparent bands. The structures of intermediate states ① and ③ and transition state ② are shown. The ADP molecule is shown in the vdW mode. The residues surrounding ADP are shown in sticks (positively charged ones in blue, negatively charged ones in red, polar residues in green, and nonpolar ones in gray). The Mg^{2+} ion is shown as a yellow sphere. ADP binds deeply inside the pocket and interacts with several polar residues in intermediate ①. The high free energy barrier is caused by the bond-breaking between ADP and Mg^{2+}.

https://doi.org/10.1021/jacs.4c09528
J. Am. Chem. Soc. 2024, 146, 28360−28374

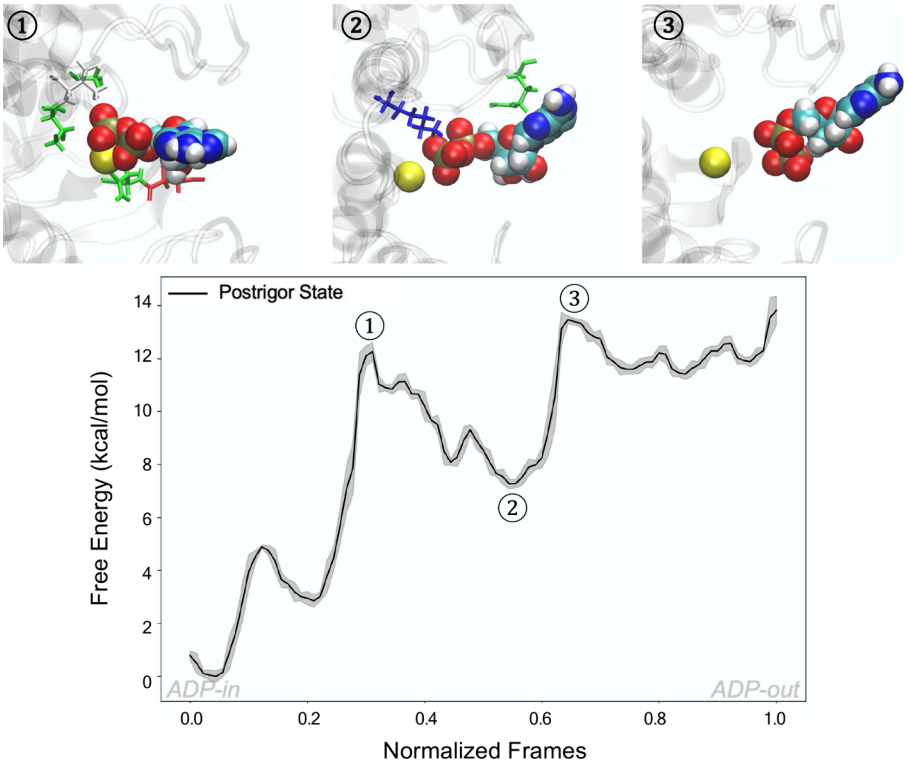

Figure 9. Free energy profile (by the TAPS method) along the minimum free energy path of ADP release from the postrigor state of myosin V. The *x*-axis is labeled by normalized simulation frame numbers, with error bars shown as transparent bands. The structures of the intermediate states ② and the transition states ① and ③ are shown. The ADP molecule is shown in vdW mode. The residues surrounding ADP are shown in sticks (positively charged ones in blue, negatively charged ones in red, polar residues in green, and nonpolar ones in gray). Mg^{2+} is shown as a yellow sphere. The ADP has a shallow binding position. It is easier for ADP to break its bonds with the Mg^{2+} and the surrounding polar residues.

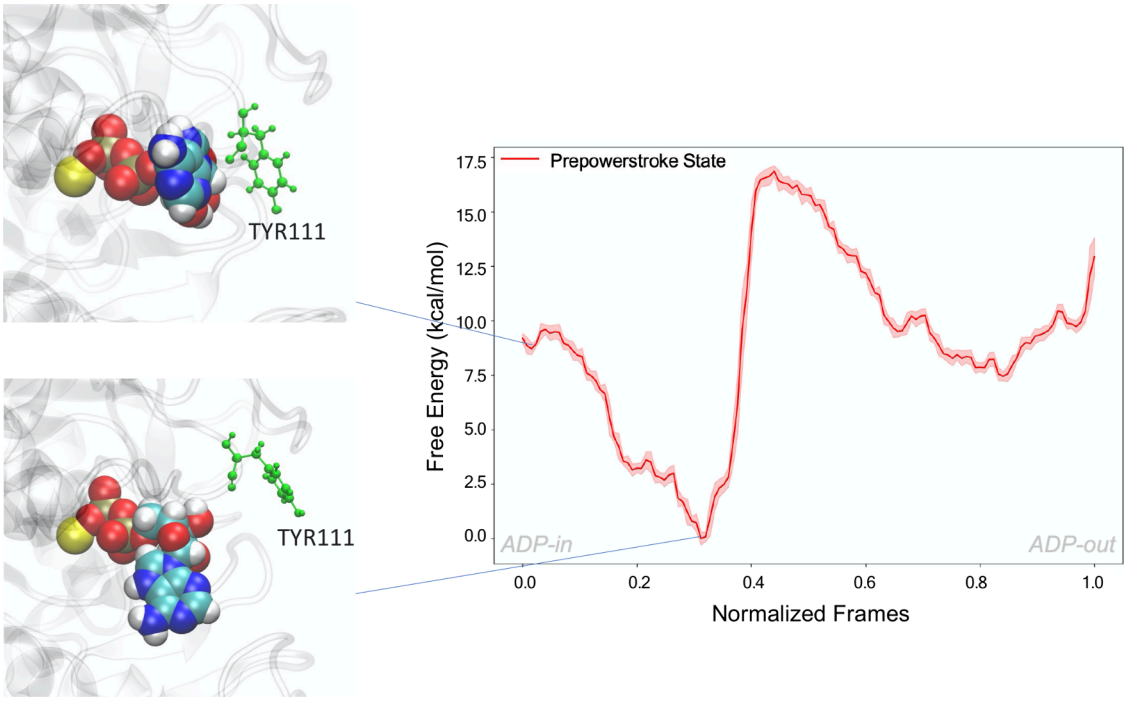

Figure 10. Structural analysis of the path for ADP release from the prepowerstroke state of myosin V. The *x*-axis is labeled by normalized simulation frame numbers with error bars shown as transparent bands. The ADP molecule is shown in vdW mode. TYR111 is shown in CPK mode. In the prepowerstroke state, the ADP undergoes a significant downward flip of the benzene ring before its release. Due to the deep location of the ADP binding, the loop above the pocket (represented by TYR111) tightly closes the exit. The ADP tends to push the loop away to open the pocket.

https://doi.org/10.1021/jacs.4c09528
J. Am. Chem. Soc. 2024, 146, 28360−28374

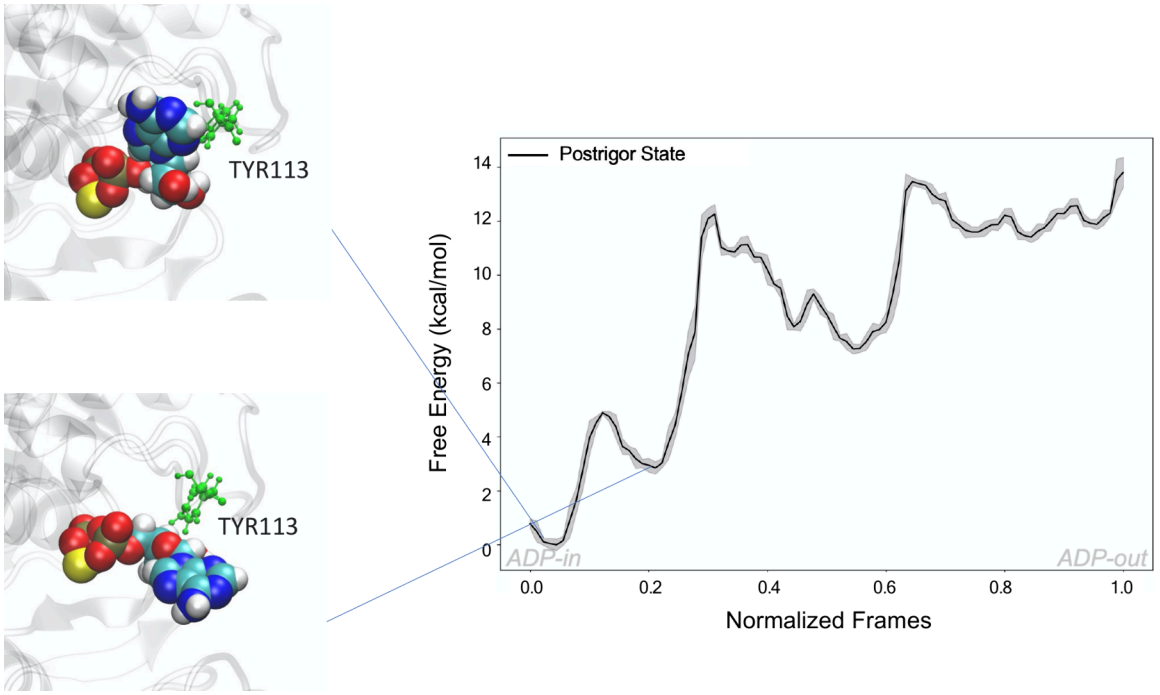

Figure 11. Structural analysis of the path for the ADP release from the postrigor state of myosin V. The *x*-axis is labeled by normalized simulation frame numbers, with error bars shown as transparent bands. The ADP molecule is shown by vdW representation. TYR113 (corresponding to TYR111 in 4zg4.pdb) is shown in the CPK mode. In the postrigor state, the tyrosine (TYR113) has been squeezed to the side due to the shallow binding position of the ADP, resulting in a bigger space in the pocket opening for the ADP to exit. Therefore, ADP does not need to be flipped significantly.

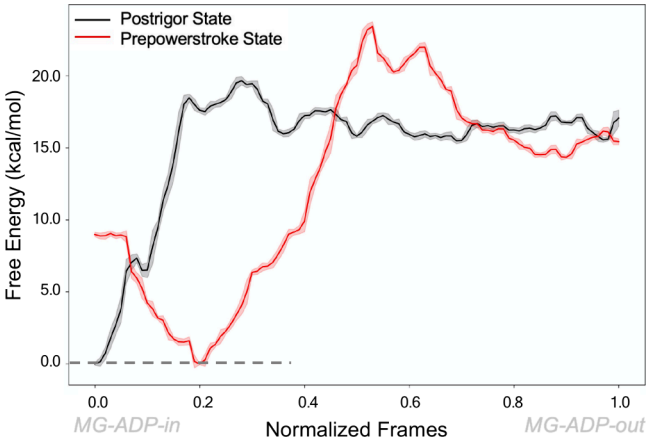

Figure 12. TAPS results for the MG-ADP release from the postrigor and prepowerstroke states of myosin V. The *x*-axis is labeled by normalized simulation frame numbers. The "zero" value corresponds to the MG-ADP bound state, and the "one" value corresponds to the MG-ADP unbound state. The error bars are shown as transparent bands. The free energy barrier for releasing MG-ADP in the postrigor state is lower compared to that in the prepowerstroke state.

umbrella sampling-based free energy simulation by considering the distance between myosin and ADP as an order parameter (Figure 6) in our free energy profile. At a lower distance, the ADP is bound to myosin, whereas at a higher distance, the ADP becomes unbound from myosin. The most stable minima in the free energy profile corresponds to the ADP bound state to myosin V. From our free energy analysis, we have found that the ADP release from the postrigor state is easier than the prepowerstroke state of myosin V. This result is in accordance with our SMD simulation results as well as earlier experimental findings. It is interesting to note that in the case of the prepowerstroke state (leading end) of myosin V, the location of ADP is deep inside the binding pocket and the exit of ADP is tightly closed by a tyrosine at the 111th position whereas in the case of the postrigor state of myosin V, the ADP has a shallow binding position, which causes a bigger space for ADP release, and the tyrosine at the 113th position (corresponding to the 111th position of the prepowerstroke state of myosin V) does not hinder the exit of ADP as was the case in the prepowerstroke state of myosin V. Thus, the ADP release is easier from the postrigor state of myosin V compared to its prepowerstroke state. It will be discussed in more detail in the TAPS simulation discussion section below.

3.4. TAPS Simulation of Myosin V. To understand the mechanism of ADP release from myosin V, we used the TAPS method to locate the MFEP connecting the ADP-bound state and the ADP-unbound state of myosin V. The free energy profiles along the MFEPs (Figure 7), obtained by TAPS simulations, reveal that the postrigor state is more likely to release ADP than the prepowerstroke state, consistent with the above results. The detailed mechanism of release can be illustrated by the structures of the transition state and intermediate state along the MFEP. In the prepowerstroke state of myosin V, the location of ADP is deep inside the binding pocket and surrounded by polar residues. The high free energy barrier is caused by the bond-breaking between ADP and Mg^{2+} (Figure 8). By contrast, in the postrigor state of myosin V, the ADP has a shallow binding region. The free energy barrier is lower, and ADP breaks its bonds with Mg^{2+} and the surrounding polar residues easier (Figure 9).

It is interesting to note that, in the prepowerstroke state, the exit of ADP is tightly closed by a tyrosine at the 111th position. To open the exit, ADP undergoes a significant downward flip

https://doi.org/10.1021/jacs.4c09528
J. Am. Chem. Soc. 2024, 146, 28360−28374

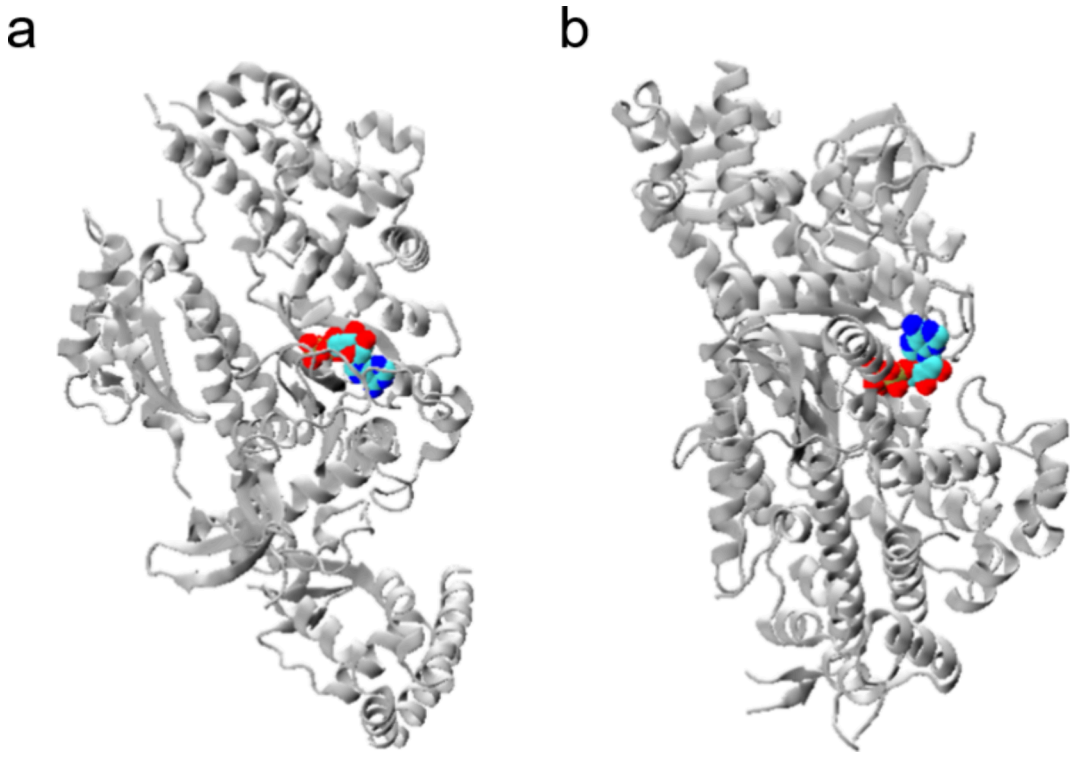

Figure 13. Structures of myosin VI in a cartoon representation. (a) Postrigor state of myosin VI. The attached ADP is shown by vdW representation. (b) Prepowerstroke state of myosin VI with ADP. The structures of postrigor conformation and prepowerstroke conformation have been taken from the Protein Data Bank having PDB ID 2vb6.pdb and 2v26.pdb, respectively.

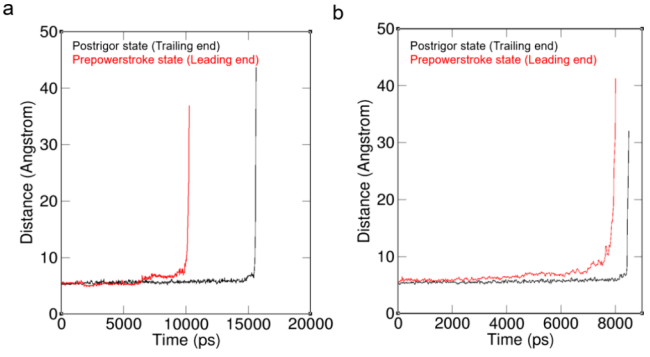

Figure 14. SMD simulation results for myosin VI at different conformations. Here, the ADP-myosin distance has been plotted with time. At a lower distance, ADP and myosin are attached to each other whereas at a higher distance, they are dissociated from each other. (a) SMD results of the ADP dissociation from myosin VI at postrigor and prepowerstroke conformation at force constant 0.004 kcal mol^{-1} $Å^{-2}$. (b) SMD results of the ADP dissociation from myosin VI at postrigor and prepowerstroke conformation at force constant 0.009 kcal mol^{-1} $Å^{-2}$.

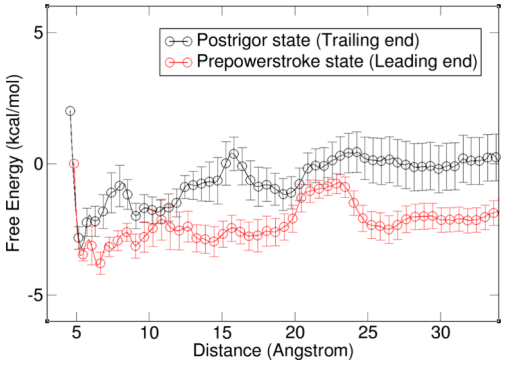

Figure 15. Umbrella sampling simulation results of myosin VI at the postrigor and prepowerstroke conformations. Here, the free energy is plotted by considering the distance between the ADP molecule and myosin as an order parameter. Note that the postrigor state has a higher energy barrier from the ADP bound (to myosin) to the ADP-dissociated state whereas the prepowerstroke state has a lower energy barrier. The most stable minima in the above free energy profile corresponds to the ADP-bound state with myosin. The error bars were calculated by bootstrapping.

of the benzene ring (Figure 10). However, in the postrigor state, the tyrosine at the 113th position (corresponding to the 111th position in 4zg4.pdb) has been squeezed to the side, due to the shallow binding region of the ADP, making no hindrance for the exit of ADP and offering a bigger space for ADP release (Figure 11). Therefore, the ADP release is easier from the postrigor state of myosin V compared to its prepowerstroke state.

During the simulations, we noticed the tight bond between ADP and Mg^{2+}. This bond raises another possibility that Mg^{2+} may be released along with ADP. Therefore, the TAPS approach and free energy calculation were also performed for this case. It is important to mention that a kinetic assay experimental study indicates the Mg^{2+} inhibits the ADP release rate constant in the subset of myosin examined, and also the Mg^{2+}-dependent regulation of motor activity is conserved in myosin motors.[68] Overall, these experimental results suggest that the Mg^{2+} ion reduces the ADP release rate constant and rate of attachment to actin in both high and low duty ratio myosin. Another experimental study[69] shows that for myosin V and myosin VI, increasing the magnesium concentration would

https://doi.org/10.1021/jacs.4c09528
J. Am. Chem. Soc. 2024, 146, 28360−28374

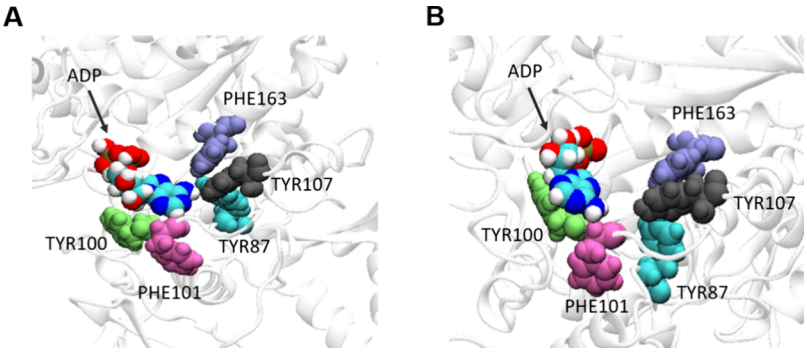

Figure 16. Structural analysis of the simulation snapshots of the distribution of hydrophobic amino acids around the ADP molecule of myosin VI. (A) Distribution of hydrophobic phenylalanine and tyrosine around the ADP in the case of the postrigor state (trailing end) of myosin VI. (B) Distribution of those hydrophobic amino acids around the ADP for the prepowerstroke state (leading end) of myosin VI.

Table 1. Summary of the Difference of the ADP Release Barrier between the Leading and Trailing Ends (D_{L-T}) of Myosins V and VI from Simulation and Experimental Observation

system	D_{L-T}(TAPS) kcal/mol	D_{L-T}(renormalization) kcal/mol	D_{L-T}(umbrella) kcal/mol	D_{L-T}(expt)[70,71,73a] kcal/mol
myosin V	5	3	5	2.7
myosin VI	−3	−5	−2	−0.5

[a]Experimental barriers are extracted by using the Eyring transition state equation from the reported rate.

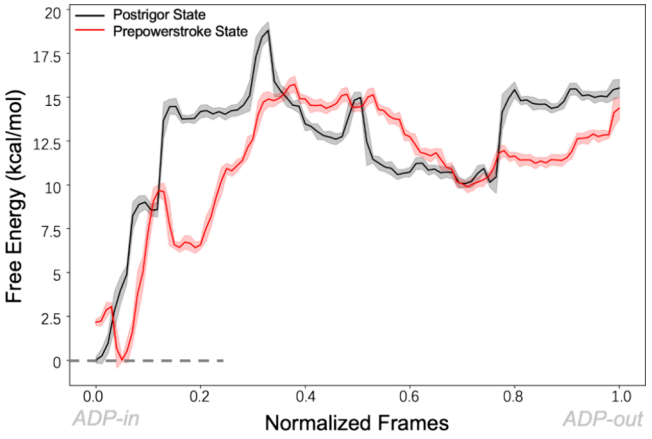

Figure 17. TAPS results for the ADP release from the postrigor and prepowerstroke states of myosin VI. The *x*-axis is labeled by normalized simulation frame numbers. The "zero" value corresponds to the ADP-bound state, and the "one" value corresponds to the ADP-unbound state. The error bars are shown as transparent bands. The free energy barrier for releasing ADP in the postrigor state is higher compared to the prepowerstroke state.

be predicted to slow the steady-state ATPase rate, because the ADP release is rate-limiting. It is worth mentioning that we also demonstrated the effect of Mg^{2+} on the ADP release using the TAPS method. The corresponding free energy profile (Figure 12) shows that the release of the MG-ADP system is also easier from the postrigor state than from the prepowerstroke state of myosin V (which is also true when we consider ADP release alone). Notably, the free energy barriers are higher in both conformations for the MG-ADP system compared to the case of corresponding ADP release. It suggests that the two states (prepowerstroke and postrigor) of myosin V prefer to release ADP alone.

3.5. SMD Simulation of Myosin VI. Next, we checked the ADP release propensities of different conformations of myosin VI. Myosin VI is the only member in the myosin family that exhibits reverse directionality. It could be fascinating to explore the energetics of different conformations of myosin VI, as we already performed the same for myosin V in previous sections. To understand how the ADP dissociation occurs from different states of myosin VI, we first accomplished an SMD simulation and monitored the distance between the ADP and myosin VI with time. We considered both the postrigor and prepowerstroke conformations of myosin VI to understand the ADP dissociation from them as we did for myosin V. The postrigor conformation and prepowerstroke conformation of myosin VI have been reported in the available crystal structure (Figure 13) in the Protein Data Bank (PDB) and used here in our simulations. The PDB ID of postrigor and prepowerstroke conformations of myosin VI used here are 2vb6 and 2v26, respectively. As shown from the SMD simulation (Figure 14), at lower distances, the ADP is bound with myosin whereas as distance increases, the ADP gets dissociated from myosin VI. We have found that in the case of myosin VI, the ADP release is slower from postrigor conformation whereas it is relatively faster from the prepowerstroke conformation of myosin VI (Figure 14a,b). We checked with two different force constants 0.004 and 0.009 kcal mol^{-1} $Å^{-2}$ (Figure 14a,b), and in both cases, we found a similar trend. It indicates that ADP dissociates less favorably from the postrigor state of myosin VI compared to its prepowerstroke conformation (Supplementary Movies 3 and 4). It is important to note that this trend is reverse when compared to myosin V. It indicates that energetics might play an important role behind the reverse directionality of myosin VI compared to myosin V. However, to acquire a detailed energetic insight of the ADP dissociation from these states, we have accomplished free energy analysis with postrigor and prepowerstroke conformations of myosin VI in the next sections.

3.6. Renormalization Simulations of Myosin VI. The renormalization approach was also applied to myosin VI. Here again, we obtained a nice trend between MD and LD results using barriers of 11−12 kcal/mol for the leading end and 15−17 kcal/mol for the trailing end (Figures S4 and S5). These results are similar to the TAPS results reported below,

https://doi.org/10.1021/jacs.4c09528
J. Am. Chem. Soc. 2024, 146, 28360−28374

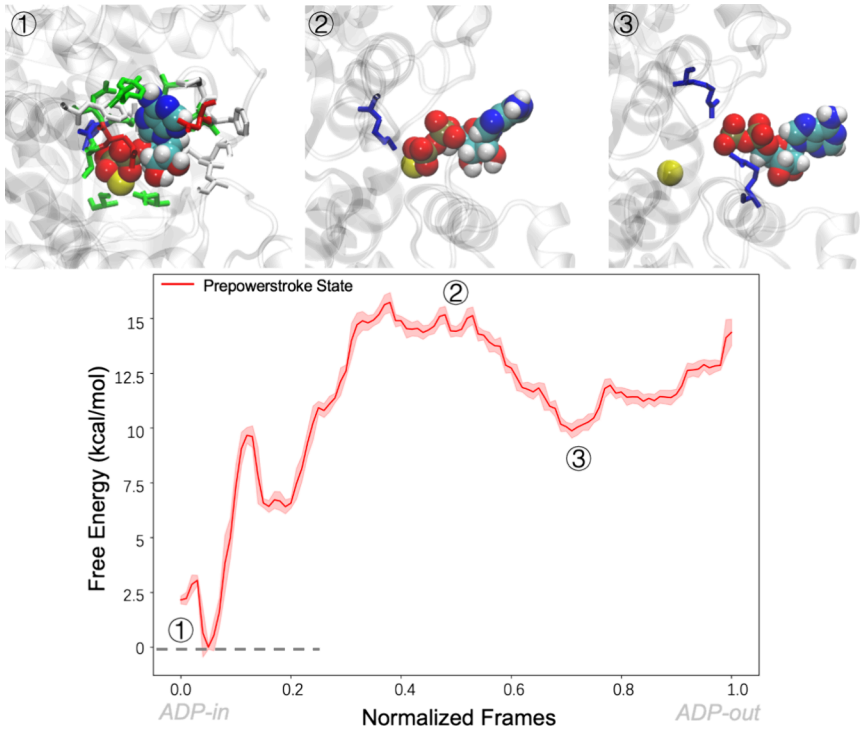

Figure 18. TAPS free energy profile along the minimum free energy path of the ADP release from the prepowerstroke state of myosin VI. The *x*-axis is labeled by normalized simulation frame numbers of the MFEP, with error bars shown as transparent bands. The structures of the intermediate states ① and ③ and the transition state ② are shown. The ADP molecule is shown in the vdW mode. The residues surrounding the ADP are shown in sticks (positively charged ones in blue, negatively charged ones in red, polar residues in green, and nonpolar ones in gray). Mg^{2+} is shown as a yellow sphere.

confirming that in myosin VI, the trailing end has a higher barrier of ADP release compared to its leading end.

3.7. Umbrella Sampling Simulation of Myosin VI. From the renormalization simulations of myosin VI, we have found that the ADP release from the postrigor state is less feasible than the prepowerstroke state. To reexamine this result, we have now performed umbrella sampling simulation by considering the distance between myosin VI and the ADP as an order parameter (Figure 15). At a lower distance, ADP and myosin VI are bound, whereas at a higher distance, they dissociated from each other. The most stable minima in this free energy profile correspond to the ADP bound state to myosin VI. As evident from our free energy analysis, the ADP release from the postrigor state is less favorable than the same from the prepowerstroke state. The simulations indicated that in the case of myosin VI, some hydrophobic amino acid (tyrosine and phenyl alanine) residues extensively shielded the ADP molecule at the postrigor state (Figure 16A). Those residues are Tyrosine 87, Tyrosine 100, Phenylalanine 101, Tyrosine 107, and Phenylalanine 163. The ADP molecules are buried inside these hydrophobic residues in the postrigor state of myosin VI; releasing the ADP from such strong hydrophobic environments requires greater energetic cost. On the other hand, as evident from our simulations, in the case of the prepowerstroke state of myosin VI, the ADP is mostly shielded by Tyrosine 100 and Phenylalanine 101 but does not interact extensively with Tyrosine 87, Tyrosine 107, and Phenylalanine 163 (Figure 16B), and thus release of the ADP from the prepowerstroke state of myosin VI requires less energetic cost compared to the postrigor state of myosin VI. Table 1 indicates the difference in free energy barrier of ADP release from the leading to trailing ends of myosin V and VI. It is evident from the table that for myosin V, the ADP release from the leading end impedes compared to its trailing end, whereas for myosin VI, the ADP release from the trailing end impedes compared to its leading end. This trend matches earlier experimental studies.[70−73] It is important to mention that for myosin V, the experimentally observed ADP release rate from the leading end is 0.16 s^{-1} and that for the trailing end is 14 s^{-1}, where the ADP release from the leading end is rate limiting for myosin V.[70,71] On the other hand, the experimentally observed ADP release rate from the trailing end of myosin VI is 5.5 s^{-1} and it is rate limiting, whereas the combination of all other steps of myosin VI gives a rate of 11 s^{-1}.[73]

3.8. TAPS Simulation of Myosin VI. The free energy profiles along the MFEPs (Figure 17), obtained by TAPS simulations, reveal that the prepowerstroke state is more likely to release ADP than the postrigor state, consistent with the above results. The detailed mechanism of release can be illustrated by the structures of the transition state and intermediate states along the MFEP. In the prepowerstroke state of myosin VI, the ADP is buried inside some polar residues. The acidic amino acids at the entrance may help the ADP release (Figure 18). By contrast, in the postrigor state of myosin VI, the ADP is surrounded by extra residues with large side chains (such as TYR87 and TYR107). The residues create additional obstacles to the release of the ADP. The high free energy barrier is mainly caused by the flipping-out of the ADP (Figure 19).

Overall, the most reliable results are obtained by the TAPS method, where the activation barriers are 17.5 and 12.5 kcal/mol, for the myosin V leading and trailing ends, respectively. The corresponding observed values are 18.7 and 16 kcal/mol, respectively. The corresponding barriers obtained from the

https://doi.org/10.1021/jacs.4c09528
J. Am. Chem. Soc. 2024, 146, 28360−28374

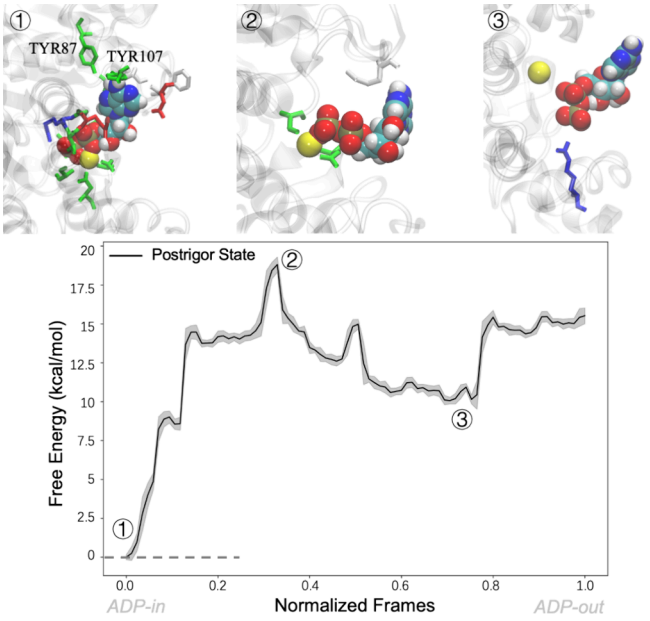

Figure 19. Free energy profile (by the TAPS method) along the minimum free energy path of ADP release from the postrigor state of myosin VI. The *x*-axis is labeled by normalized simulation frame numbers, with error bars shown as transparent bands. The structures of the initial state ①, the transition state ②, and the intermediate state ③ are shown. The ADP molecule is shown in vdW mode. The residues surrounding the ADP are shown in sticks (positively charged ones in blue, negatively charged ones in red, polar residues in green, and nonpolar ones in gray). Mg^{2+} is shown as a yellow sphere. The ADP is surrounded by more residues with large side chains (such as TYR87 and TYR107) in the initial state ①. The high free energy barrier is mainly caused by the flipping-out of the ADP.

renormalization approach are 20 and 17 kcal/mol, respectively, while the results for the umbrella sampling simulations are 11 and 6 kcal/mol, respectively. The barriers obtained by the umbrella sampling method significantly underestimated the observed barriers. In the case of myosin VI, the TAPS barriers for the leading and trailing ends are 15 and 18 kcal/mol, respectively, as compared to observed barriers of 16.1 and 16.6, kcal/mol, respectively. The corresponding barriers obtained by the renormalization simulations are 12 and 17 kcal/mol, while the results for the umbrella sampling simulations are again underestimated, with values of 2 and 4 kcal/mol, respectively.

However, our main point is that the difference between the forward and backward barriers is nicely captured by our three approaches and in all cases reproduce the experimentally observed rate, and as mentioned above, the corresponding values of the barriers are given in Table 1.

4. CONCLUDING REMARKS

This work focuses on establishing the origin of the unidirectionality of myosin. Following our more tentative earlier study,[22] where it was concluded that the barrier for the rate-limiting ADP release step controls the directionality, here we performed systematic evaluations of the barrier for ADP release in the forward and backward paths. Considering the major convergence problems, we explored the barrier by approaches with different levels of reliability, ranging from the renormalization method to the automated path searching method. Our studies tend to explore how the energy landscape of the ADP release from different conformations of myosin V and myosin VI vary for the forward and backward motions. Hence, the ADP release energetics from different conformations of myosin is definitely related to the directionality of myosin motors. All our simulation approaches reproduce the observed trend, where the ADP is released faster from the postrigor state or rear end (which is in the lever-down conformation) of myosin V, whereas in the case of myosin VI, the ADP is released faster from the prepowerstroke state (leading end) compared to its postrigor state (rear end). Such finding about myosin motor protein is also consistent with the experimental observations.[71−76]

Recently, free energy-based simulation studies have been employed to understand structural and dynamical changes in motor protein.[77,78] Such free energy-based simulations (e.g., ref 77) indicate that the free energy landscape of myosin VI exhibits a low free energy transition tube, which enables to connect the postrigor state to a putative transition state (PTS). This observation indicates that the PTS is kinetically accessible from a postrigor state and supports the hypothesis that it is an on-pathway intermediate along the recovery stroke. Their results indicated that the initial step of the converter-initiated scenario is much faster as compared to any Switch II-initiated mechanism, at least in the case of myosin VI. Several other works also indicated how free energy-based studies could be pivotal for different other motor proteins.[79,80] We would like to note that our earlier extensive free energy studies[81−84] including coarse-grained simulations have not only provided a rather clear picture on the conversion of chemical energy to mechanical energy by motor proteins but also indicated that this key process follows microscopic reversibility[85] and does not involve dynamical effects.

We also identified the molecular origin of the difference in energetics of the ADP release from different conformations of myosin V and myosin VI. It has been concluded that the organization of specific hydrophobic amino acid residues (phenylalanine and tyrosine) close to the ADP binding groove of myosin plays a significant role behind their difference in the ADP release energetics.

As is evident, comparing the barriers obtained using different approaches could be a topic of interest from a methodological point of view and requires further studies. However, they are not the point of the present study, where we would like to show that the trend of the calculated differences between the ADP release barriers is reproduced by all the methods, and thus, the umbrella sampling and renormalization method can be used in related future studies. It is possible that the umbrella sampling approach misses the equivalent of the nonequilibrium solvation barrier[86] and thus underestimates the correct barrier.

Structurally, one of the major differences between myosins V and VI lies in their neck domains: The neck region of myosin V consists of six light-chain binding sites (IQ motifs) bound with six calmodulins (CAM), whereas in the case of myosin VI, it has a short linker consisting only of one IQ motif bound with one CAM.[87] An important point to mention in this context is that in the case of myosin V, due to intramolecular strain, the lever arm of the lead head cannot complete its swing and thus the ADP release from the prepowerstroke state or lever-up state (corresponding to the leading end)[22] is greatly slowed, which is evident from experimental findings.[88] While this is slowed down, the ADP could be rapidly dissociated from the postrigor state or lever-down state (rear end),[22] therefore allowing the ATP to bind rapidly and then dissociate the rear head from the actin track, which leads to forward stepping of

https://doi.org/10.1021/jacs.4c09528
J. Am. Chem. Soc. 2024, 146, 28360−28374

myosin V. This phenomenon has been directly witnessed experimentally by visualizing an approximate 70° swing of the lever arm[89,90] of the stepping myosin V dimer. This is also evident from our current study. On the other hand, in contrast with myosin V, the leading head of a myosin VI dimer walking on the actin track releases the ADP at a rate that is the same as in absence of the strain, i.e., its motion is totally strain independent.[91] Instead of slowing down the ADP release from the leading end of myosin VI, gating of the leading head in myosin VI is fulfilled by preventing rapid binding of ATP.[91] Our current study is also consistent with these experimental findings, which indicates that the ADP release from the leading end (compared to trailing end) of myosin VI is not slowed down as we found in the case of myosin V.

■ ASSOCIATED CONTENT

Data Availability Statement

The processed data generated in this study such as the example of input files and structural data, scripts, and sample simulation trajectories were provided in the data repositories (https://github.com/ritaban368/Myosin_project). Additional sample simulation trajectories of the systems studied here are shown in Supplementary Movies 1−4.

Supporting Information

The Supporting Information is available free of charge at https://pubs.acs.org/doi/10.1021/jacs.4c09528.

Convergence test of the simulations; atom sets for RMSD calculations; and renormalization of myosin V (leading end), myosin VI (trailing end), and myosin VI (leading end) (PDF)

ADP dissociation from the postrigor state of myosin V - Supplementary Movie 1 (MP4)

ADP dissociation from the prepowerstroke state of myosin V - Supplementary Movie 2 (MP4)

ADP dissociation from the postrigor state of myosin VI - Supplementary Movie 3 (MP4)

ADP dissociation from the prepowerstroke state of myosin VI - Supplementary Movie 4 (MP4)

■ AUTHOR INFORMATION

Corresponding Author

Arieh Warshel − *Department of Chemistry, University of Southern California, Los Angeles, California 90089-1062, United States;* orcid.org/0000-0001-7971-5401; Email: warshel@usc.edu

Authors

Ritaban Halder − *Department of Chemistry, University of Southern California, Los Angeles, California 90089-1062, United States;* orcid.org/0000-0002-0872-6522

Zhen Tao Chu − *Department of Chemistry, University of Southern California, Los Angeles, California 90089-1062, United States*

Rujuan Ti − *Warshel Institute for Computational Biology, School of Medicine, The Chinese University of Hong Kong, Shenzhen, Guangdong 518172, China;* orcid.org/0000-0002-5169-8491

Lizhe Zhu − *Warshel Institute for Computational Biology, School of Medicine, The Chinese University of Hong Kong, Shenzhen, Guangdong 518172, China;* orcid.org/0000-0001-8252-7807

Complete contact information is available at: https://pubs.acs.org/10.1021/jacs.4c09528

Notes

The authors declare no competing financial interest.

■ ACKNOWLEDGMENTS

We thank the University of Southern California, Center of High-Performance Computing (HPC), for computational resources. This work was supported by the National Science Foundation Grant MCB-1707167 and the National Institute of Health Grant R35 GM122472.

■ REFERENCES

(1) Sweeney, H. L.; Holzbaur, E. L. F. Motor Proteins. *Cold Spring Harb Perspect Biol.* **2018**, *10*, a021931.

(2) Hirokawa, N.; Noda, Y.; Tanaka, Y.; Niwa, S. Kinesin superfamily motor proteins and intracellular transport. *Nat. Rev. Mol. Cell Biol.* **2009**, *10*, 682−696.

(3) Goldstein, L. S. B. Kinesin molecular motors: Transport pathways, receptors, and human disease. *Proc. Natl. Acad. Sci. U.S.A.* **2001**, *98*, 6999−7003.

(4) Canty, J. T.; Tan, R.; Kusakci, E.; Fernandes, J.; Yildiz, A. Structure and Mechanics of Dynein Motors. *Annu. Rev. Biophys* **2021**, *50*, 549−574.

(5) Roberts, A. J.; Kon, T.; Knight, P. J.; Sutoh, K.; Burgess, S. A. Functions and mechanics of dynein motor proteins. *Nat. Rev. Mol. Cell Biol.* **2013**, *14*, 713−726.

(6) Tafoya, S.; Bustamante, C. Molecular switch-like regulation in motor proteins. *Philos. Trans. R. Soc. B* **2018**, *373*, No. 20170181.

(7) Anderson, E. N.; White, J. A.; Gunawardena, S. Axonal transport and neurodegenerative disease: vesicle-motor complex formation and their regulation. *Degener Neurol Neuromuscul Dis* **2014**, *4*, 29−47.

(8) Brady, S. T.; Morfini, G. A. Regulation of motor proteins, axonal transport deficits and adult-onset neurodegenerative diseases. *Neurobiol Dis* **2017**, *105*, 273−282.

(9) Tabassum, G.; et al. Investigating the role of Kinesin family in lung adenocarcinoma via integrated bioinformatics approach. *Sci. Rep.* **2023**, *13*, 9859.

(10) Ménasché, G.; et al. Griscelli syndrome restricted to hypopigmentation results from a melanophilin defect (GS3) or a MYO5A F-exon deletion (GS1). *J. Clin Invest* **2003**, *112*, 450−456.

(11) Pylypenko, O.; et al. Myosin VI deafness mutation prevents the initiation of processive runs on actin. *Proc. Natl. Acad. Sci. U. S. A.* **2015**, *112*, No. E1201.

(12) Sato, O.; et al. Human Deafness Mutation of Myosin VI (C442Y) Accelerates the ADP Dissociation Rate. *J. Biol. Chem.* **2004**, *279*, 28844−28854.

(13) Hurd, D. D.; Saxton, W. M. Kinesin mutations cause motor neuron disease phenotypes by disrupting fast axonal transport in Drosophila. *Genetics* **1996**, *144*, 1075−1085.

(14) Martinez-Carrera, L. A.; Wirth, B. Dominant spinal muscular atrophy is caused by mutations in BICD2, an important golgin protein. *Front. Neurosci.* **2015**, *9*, 401.

(15) Eschbach, J.; Dupuis, L. Cytoplasmic dynein in neurodegeneration. *Pharmacol Ther* **2011**, *130*, 348−363.

(16) Duke, T. Push or pull? Teams of motor proteins have it both ways. *Proc. Natl. Acad. Sci. U. S. A.* **2002**, *99*, 6521−6523.

(17) Wade, R. H.; Kozielski, F. Structural links to kinesin directionality and movement. *Nat. Struct Mol. Biol.* **2000**, *7*, 456−460.

(18) Woehlke, G.; Schliwa, M. Directional motility of kinesin motor proteins. *Biochimica et Biophysica Acta (BBA) - Molecular Cell Research* **2000**, *1496*, 117−127.

(19) Can, S.; Lacey, S.; Gur, M.; Carter, A. P.; Yildiz, A. Directionality of dynein is controlled by the angle and length of its stalk. *Nature* **2019**, *566*, 407−410.

(20) Cappello, G.; et al. Myosin V stepping mechanism. *Proc. Natl. Acad. Sci. U.S.A.* **2007**, *104*, 15328−15333.

(21) Jana, B.; Onuchic, J. N. Strain Mediated Adaptation Is Key for Myosin Mechanochemistry: Discovering General Rules for Motor Activity. *PLoS Comput. Biol.* **2016**, *12*, No. e1005035.
(22) Alhadeff, R.; Warshel, A. Reexamining the origin of the directionality of myosin V. *Proc. Natl. Acad. Sci. U.S.A.* **2017**, *114*, 10426−10431.
(23) Mukherjee, S.; Warshel, A. Electrostatic origin of the unidirectionality of walking myosin V motors. *Proc. Natl. Acad. Sci. U. S. A.* **2013**, *110*, 17326−17331.
(24) Pertici, I.; et al. A myosin II nanomachine mimicking the striated muscle. *Nat. Commun.* **2018**, *9*, 3532.
(25) Ni, Q.; et al. A tug of war between filament treadmilling and myosin induced contractility generates actin rings. *Elife* **2022**, *11*, No. e82658.
(26) De La Cruz, E. M.; Wells, A. L.; Rosenfeld, S. S.; Ostap, E. M.; Sweeney, H. L. The kinetic mechanism of myosin V. *Proc. Natl. Acad. Sci. U.S.A.* **1999**, *96*, 13726−13731.
(27) Yengo, C. M.; De La Cruz, E. M.; Safer, D.; Ostap, E. M.; Sweeney, H. L. Kinetic Characterization of the Weak Binding States of Myosin V. *Biochemistry* **2002**, *41*, 8508−8517.
(28) Smith, D.; Sleep, J. Strain-Dependent Kinetics of the Myosin Working Stroke, and How They Could Be Probed with Optical-Trap Experiments. *Biophys. J.* **2006**, *91*, 3359−3369.
(29) Trybus, K. M.; Krementsova, E.; Freyzon, Y. Kinetic Characterization of a Monomeric Unconventional Myosin V Construct. *J. Biol. Chem.* **1999**, *274*, 27448−27456.
(30) Baker, J. E.; et al. Myosin V processivity: Multiple kinetic pathways for head-to-head coordination. *Proc. Natl. Acad. Sci. U.S.A.* **2004**, *101*, 5542−5546.
(31) Ciocanel, M.-V.; et al. Simulated actin reorganization mediated by motor proteins. *PLoS Comput. Biol.* **2022**, *18*, No. e1010026.
(32) Lan, G.; Sun, S. X. Dynamics of Myosin-V Processivity. *Biophys. J.* **2005**, *88*, 999−1008.
(33) Tehver, R.; Thirumalai, D. Rigor to Post-Rigor Transition in Myosin V: Link between the Dynamics and the Supporting Architecture. *Structure* **2010**, *18*, 471−481.
(34) Yu, H.; Ma, L.; Yang, Y.; Cui, Q. Mechanochemical Coupling in the Myosin Motor Domain. I. Insights from Equilibrium Active-Site Simulations. *PLoS Comput. Biol.* **2007**, *3*, No. e21.
(35) Masuda, T. Molecular dynamics simulation of a myosin subfragment-1 docking with an actin filament. *Biosystems* **2013**, *113*, 144−148.
(36) Patel, J. S.; Berteotti, A.; Ronsisvalle, S.; Rocchia, W.; Cavalli, A. Steered Molecular Dynamics Simulations for Studying Protein−Ligand Interaction in Cyclin-Dependent Kinase 5. *J. Chem. Inf. Model.* **2014**, *54*, 470−480.
(37) Skovstrup, S.; David, L.; Taboureau, O.; Jørgensen, F. S. A steered molecular dynamics study of binding and translocation processes in the GABA transporter. *PLoS One* **2012**, *7*, No. e39360.
(38) Park, S.; Schulten, K. Calculating potentials of mean force from steered molecular dynamics simulations. *J. Chem. Phys.* **2004**, *120*, 5946−5961.
(39) Coureux, P.-D.; Sweeney, H. L.; Houdusse, A. Three myosin V structures delineate essential features of chemo-mechanical transduction. *EMBO J.* **2004**, *23*, 4527−4537.
(40) Wulf, S. F.; et al. Force-producing ADP state of myosin bound to actin. *Proc. Natl. Acad. Sci. U. S. A.* **2016**, *113*, E1844−1852.
(41) Ménétrey, J.; et al. The post-rigor structure of myosin VI and implications for the recovery stroke. *EMBO J.* **2008**, *27*, 244−252.
(42) Ménétrey, J.; Llinas, P.; Mukherjea, M.; Sweeney, H. L.; Houdusse, A. The structural basis for the large powerstroke of myosin VI. *Cell* **2007**, *131*, 300−308.
(43) Hess, B.; Kutzner, C.; Van Der Spoel, D.; Lindahl, E. GROMACS 4: Algorithms for Highly Efficient, Load-Balanced, and Scalable Molecular Simulation. *J. Chem. Theory Comput.* **2008**, *4*, 435−447.
(44) Huang, J.; MacKerell, A. D. CHARMM36 all-atom additive protein force field: validation based on comparison to NMR data. *J. Comput. Chem.* **2013**, *34*, 2135−2145.
(45) Vanommeslaeghe, K.; et al. CHARMM general force field: A force field for drug-like molecules compatible with the CHARMM all-atom additive biological force fields. *J. Comput. Chem.* **2010**, *31*, 671−690.
(46) Berendsen, H. J. C.; Grigera, J. R.; Straatsma, T. P. The missing term in effective pair potentials. *J. Phys. Chem.* **1987**, *91*, 6269−6271.
(47) Nosé, S. A unified formulation of the constant temperature molecular dynamics methods. *J. Chem. Phys.* **1984**, *81*, 511−519.
(48) Hoover, W. G. Canonical dynamics: Equilibrium phase-space distributions. *Phys. Rev. A* **1985**, *31*, 1695−1697.
(49) Parrinello, M.; Rahman, A. Polymorphic transitions in single crystals: A new molecular dynamics method. *J. Appl. Phys.* **1981**, *52*, 7182−7190.
(50) Dryga, A.; Warshel, A. Renormalizing SMD: the renormalization approach and its use in long time simulations and accelerated PMF calculations of macromolecules. *J. Phys. Chem. B* **2010**, *114*, 12720−12728.
(51) Pisliakov, A. V.; Cao, J.; Kamerlin, S. C. L.; Warshel, A. Enzyme millisecond conformational dynamics do not catalyze the chemical step. *Proc. Natl. Acad. Sci. U.S.A.* **2009**, *106*, 17359−17364.
(52) Govind Kumar, V.; Polasa, A.; Agrawal, S.; Kumar, T. K. S.; Moradi, M. Binding affinity estimation from restrained umbrella sampling simulations. *Nat. Comput. Sci.* **2023**, *3*, 59−70.
(53) Tam, N. M.; Nguyen, T. H.; Ngan, V. T.; Tung, N. T.; Ngo, S. T. Unbinding ligands from SARS-CoV-2 Mpro via umbrella sampling simulations. *R. Soc. open sci.* **2022**, *9*, No. 211480.
(54) Halder, R.; Manna, R. N.; Chakraborty, S.; Jana, B. Modulation of the Conformational Dynamics of Apo-Adenylate Kinase through a π−Cation Interaction. *J. Phys. Chem. B* **2017**, *121*, 5699−5708.
(55) Halder, R.; Warshel, A. Energetic and structural insights behind calcium induced conformational transition in calmodulin. *Proteins* **2024**, *92*, 384−394.
(56) Torrie, G. M.; Valleau, J. P. Nonphysical sampling distributions in Monte Carlo free-energy estimation: Umbrella sampling. *J. Comput. Phys.* **1977**, *23*, 187−199.
(57) Kumar, S.; Rosenberg, J. M.; Bouzida, D.; Swendsen, R. H.; Kollman, P. A. THE weighted histogram analysis method for free-energy calculations on biomolecules. *I. The method. J. Comput. Chem.* **1992**, *13*, 1011−1021.
(58) Zhu, L.; et al. TAPS: A traveling-salesman based automated path searching method for functional conformational changes of biological macromolecules. *J. Chem. Phys.* **2019**, *150*, No. 124105.
(59) Xi, K.; et al. Assessing the Performance of Traveling-salesman based Automated Path Searching (TAPS) on Complex Biomolecular Systems. *J. Chem. Theory Comput.* **2021**, *17*, 5301−5311.
(60) Wang, L.; Xi, K.; Zhu, L.; Da, L.-T. DNA Deformation Exerted by Regulatory DNA-Binding Motifs in Human Alkyladenine DNA Glycosylase Promotes Base Flipping. *J. Chem. Inf. Model.* **2022**, *62*, 3213−3226.
(61) Xi, K.; Zhu, L. Automated Path Searching Reveals the Mechanism of Hydrolysis Enhancement by T4 Lysozyme Mutants. *Int. J. Mol. Sci.* **2022**, *23*, 14628.
(62) Ti, R.; et al. Fine-tuning activation specificity of G-protein-coupled receptors via automated path searching. *Proc. Natl. Acad. Sci. U. S. A.* **2024**, *121*, No. e2317893121.
(63) Tribello, G. A.; Bonomi, M.; Branduardi, D.; Camilloni, C.; Bussi, G. PLUMED 2: New feathers for an old bird. *Comput. Phys. Commun.* **2014**, *185*, 604−613.
(64) Applegate, D. L.; Bixby, R. E.; Chvátal, V.; Cook, W. J. Ed., *The traveling salesman problem: a computational study*; Princeton University Press, 2011.
(65) Bussi, G.; Donadio, D.; Parrinello, M. Canonical sampling through velocity rescaling. *J. Chem. Phys.* **2007**, *126*, No. 014101.
(66) Cox, M. A. A.; Cox, T. F. *Multidimensional Scaling" in Handbook of Data Visualization*; Springer: Berlin Heidelberg, 2008 pp. 315−347.
(67) Branduardi, D.; Gervasio, F. L.; Parrinello, M. From A to B in free energy space. *J. Chem. Phys.* **2007**, *126*, No. 054103.

https://doi.org/10.1021/jacs.4c09528
J. Am. Chem. Soc. 2024, 146, 28360−28374

(68) Swenson, A. M.; et al. Magnesium modulates actin binding and ADP release in myosin motors. *J. Biol. Chem.* **2014**, *289*, 23977−23991.
(69) Rosenfeld, S. S.; Houdusse, A.; Sweeney, H. L. Magnesium Regulates ADP Dissociation from Myosin V. *J. Biol. Chem.* **2005**, *280*, 6072−6079.
(70) Xie, P. A model for the chemomechanical coupling of myosin-V molecular motors. *RSC Adv.* **2019**, *9*, 26734−26747.
(71) Uemura, S.; Higuchi, H.; Olivares, A. O.; De La Cruz, E. M.; Ishiwata, S. Mechanochemical coupling of two substeps in a single myosin V motor. *Nat. Struct Mol. Biol.* **2004**, *11*, 877−883.
(72) Mehta, A. D.; et al. Myosin-V is a processive actin-based motor. *Nature* **1999**, *400*, 590−593.
(73) Altman, D.; Sweeney, H. L.; Spudich, J. A. The Mechanism of Myosin VI Translocation and Its Load-Induced Anchoring. *Cell* **2004**, *116*, 737−749.
(74) De La Cruz, E. M.; Ostap, E. M.; Sweeney, H. L. Kinetic Mechanism and Regulation of Myosin VI. *J. Biol. Chem.* **2001**, *276*, 32373−32381.
(75) Ménétrey, J.; et al. Processive steps in the reverse direction require uncoupling of the lead head lever arm of myosin VI. *Mol. Cell* **2012**, *48*, 75−86.
(76) Oke, O. A.; et al. Influence of lever structure on myosin 5a walking. *Proc. Natl. Acad. Sci. U.S.A.* **2010**, *107*, 2509−2514.
(77) Blanc, F. E. C.; Houdusse, A.; Cecchini, M. A weak coupling mechanism for the early steps of the recovery stroke of myosin VI: A free energy simulation and string method analysis. *PLoS Comput. Biol.* **2024**, *20*, No. e1012005.
(78) Albaugh, A.; Gingrich, T. R. Simulating a chemically fueled molecular motor with nonequilibrium molecular dynamics. *Nat. Commun.* **2022**, *13*, 2204.
(79) Golcuk, M.; Yilmaz, S. Z.; Yildiz, A.; Gur, M. The mechanism and energetics of the dynein priming stroke. *Structure* **2024**, *32*, 603−610.e4.
(80) Ito, Y.; Ikeguchi, M. Mechanism of the $\alpha\beta$ conformational change in F1-ATPase after ATP hydrolysis: free-energy simulations. *Biophys. J.* **2015**, *108*, 85−97.
(81) Bai, C.; Asadi, M.; Warshel, A. The catalytic dwell in ATPases is not crucial for movement against applied torque. *Nat. Chem.* **2020**, *12*, 1187−1192.
(82) Mukherjee, S.; Warshel, A. Dissecting the role of the γ-subunit in the rotary−chemical coupling and torque generation of F_1-ATPase. *Proc. Natl. Acad. Sci. U.S.A.* **2015**, *112*, 2746−2751.
(83) Mukherjee, S.; Bora, R. P.; Warshel, A. Torque, chemistry and efficiency in molecular motors: a study of the rotary−chemical coupling in F_1-ATPase. *Q. Rev. Biophys.* **2015**, *48*, 395−403.
(84) Mukherjee, S.; Warshel, A. Electrostatic origin of the mechanochemical rotary mechanism and the catalytic dwell of F1-ATPase. *Proc. Natl. Acad. Sci. U.S.A.* **2011**, *108*, 20550−20555.
(85) Astumian, R. D.; Mukherjee, S.; Warshel, A. The Physics and Physical Chemistry of Molecular Machines. *ChemPhysChem* **2016**, *17*, 1719−1741.
(86) Villà, J.; Warshel, A. Energetics and Dynamics of Enzymatic Reactions. *J. Phys. Chem. B* **2001**, *105*, 7887−7907.
(87) Syamaladevi, D. P.; Spudich, J. A.; Sowdhamini, R. Structural and functional insights on the Myosin superfamily. *Bioinf. Biol. Insights* **2012**, *6*, 11−21.
(88) Rosenfeld, S. S.; Lee Sweeney, H. A Model of Myosin V Processivity. *J. Biol. Chem.* **2004**, *279*, 40100−40111.
(89) Forkey, J. N.; Quinlan, M. E.; Alexander Shaw, M.; Corrie, J. E. T.; Goldman, Y. E. Three-dimensional structural dynamics of myosin V by single-molecule fluorescence polarization. *Nature* **2003**, *422*, 399−404.
(90) Toprak, E.; et al. Defocused orientation and position imaging (DOPI) of myosin V. *Proc. Natl. Acad. Sci. U.S.A.* **2006**, *103*, 6495−6499.
(91) Sweeney, H. L.; et al. How myosin VI coordinates its heads during processive movement. *EMBO J.* **2007**, *26*, 2682−2692.

https://doi.org/10.1021/jacs.4c09528
J. Am. Chem. Soc. 2024, 146, 28360−28374